Numerical study of the $E\otimes e$ Jahn-Teller polaron and bipolaron

S. El Shawish,[1] J. Bonča,[1,2] Li-Chung Ku,[3] and S. A. Trugman[3]
[1]*J. Stefan Institute, Ljubljana 1000, Slovenia*
[2]*FMF, University of Ljubljana, Ljubljana 1000, Slovenia*
[3]*Theory Division, Los Alamos National Laboratory, Los Alamos, New Mexico 87545*
(Received 6 September 2002; published 10 January 2003)

The properties of the polaron and bipolaron are explored in the one-dimensional Jahn-Teller model with dynamical quantum phonons. The ground-state properties of the polaron and bipolaron are computed using a recently developed variational method. Dynamical properties of the ground state of a polaron are investigated by calculating the optical conductivity $\sigma(\omega)$. Our numerical results suggest that the Jahn-Teller and Holstein polarons are similar. However, in the strong-coupling regime qualitative differences in $\sigma(\omega)$ between the two models are found and discussed. The influence of the electron-phonon coupling and the electrostatic repulsion on the bipolaron binding energy, bipolaron masses, and correlation functions is investigated.

DOI: 10.1103/PhysRevB.67.014301 PACS number(s): 71.38.−k, 74.20.Mn, 74.25.Kc

I. INTRODUCTION

While research on Jahn-Teller (JT) electron phonon coupling spans many decades, a renewed interest in this problem has been sparked by the discovery of colossal magnetoresistance materials (CMR). In CMR's, it is believed, the colossal magnetoresistance effect is a consequence of the interplay between the double exchange mechanism and the lattice effect.[1–4] Furthermore, recent studies of alkali-doped fullerenes A_nC_{60} indicate that the Jahn-Teller distortion, together with strong Coulomb repulsion, could be responsible for unusual electronic properties of these materials.[5–9]

Recent advances in computing capabilities have stimulated the development of various numerical techniques such as exact diagonalization techniques (ED) on small clusters,[10–12] ED on infinite clusters,[13,14] quantum Monte Carlo calculations,[15,16] variational methods,[17] and density matrix renormalization group techniques,[18] that have provided valuable results for the Holstein model (HM) in one and more spatial dimensions. The most efficient methods provide energies for the Holstein polaron problem that are accurate up to 21 digits in the thermodynamic limit.[14] In addition to static quantities, dynamic properties such as spectral functions and optical conductivity of the Holstein model have recently been studied on small lattice clusters.[19–23] However, except in the small polaron regime, such calculations are subject to pronounced finite-size effects. In contrast to the HM, there has been much less numerical research devoted to the Jahn-Teller model (JTM), mainly due to the far larger Hilbert space that presents the main obstacle to exact-diagonalization approaches. Most of the recent numerical calculations of the JTM that take into account the full quantum mechanical nature of the problem consider only one atom.[6,7] A recent path-integral quantum Monte Carlo approach, developed by Kornilovitch, has proven powerful in computing ground state and spectral properties like the density of states of the Jahn-Teller problem.[24] A calculation of dynamic properties by that method would require analytic continuation from imaginary time, which is very sensitive to statistical noise.

The scope of the present work is to compare the static properties of the JTM and HM for the case of one and two electrons. In addition, we investigate dynamic properties of the Holstein and Jahn-Teller polaron by calculating the optical conductivity. In this case we devote equal attention to the Holstein and Jahn-Teller models since dynamical properties of the Holstein model calculated using an infinite-lattice variational space have not been published elsewhere. We use a recently developed numerical technique[13,25] to study the JTM for the case of one and two electrons on a one-dimensional infinite lattice. Our main goal is to find the numerically exact solution of the JTM in the thermodynamic limit. The variational method that we use[13,25] is defined on an infinite lattice, and is not subject to finite-size effects. A standard Lanczos method is used to find ground and excited states with the selected Hilbert space. The method allows a calculation of physical properties at any wave vector k. In the intermediate coupling regime where it is most accurate, it provides results that are variational in the thermodynamic limit and gives energies accurate to 21 digits for the Holstein polaron, up to seven digits for the Holstein bound bipolaron, and six digits for the Jahn-Teller polaron. While there are no boundary finite-size effects, there are nevertheless finite-variational-space effects due to a constraint that only a finite separation between the electron and the surrounding phonons is allowed for the polaron, and between two electrons and the polaron cloud for the bipolaron. Nevertheless, results may be fairly accurate even in the two-electron case when electrons are bound into a bipolaron, since then electron-electron correlation functions decrease exponentially for large separations.

II. MODEL

The simplest, so-called $E\otimes e$ Jahn-Teller model consists of two degenerate electron orbitals and two degenerate phonon modes,

$$\begin{aligned} H=&-t\sum_{i,o,s}(c^{+}_{i+1,o,s}c_{i,o,s}+\text{ H.c.})+\omega_0\sum_i (a_i^{+}a_i+b_i^{+}b_i)\\ &+g\omega_0\sum_{i,s}[(n_{i,1,s}-n_{i,2,s})(a_i^{+}+a_i)\\ &+(c^{+}_{i,1,s}c_{i,2,s}+c^{+}_{i,2,s}c_{i,1,s})(b_i^{+}+b_i)]\\ &+U_1\sum_{i,o} n_{i,o,\uparrow}n_{i,o,\downarrow}+U_2\sum_i (n_{i,1,\uparrow}n_{i,2,\downarrow}+n_{i,2,\uparrow}n_{i,1,\downarrow}), \end{aligned} \tag{1}$$

where $c^+_{i,o,s}$ creates an electron on site i, orbital o ($o=1,2$) and spin s, and a_i^+ (b_i^+) creates dispersionless phonons of type a (b) on site i. While the phonon of type a couples to the electron density, the mode b mediates hopping between electronic orbitals that are orthogonal in the absence of phonon b. The parameters of the model are the intersite hopping matrix element t, dimensionless electron-phonon coupling strength g, and optical phonon frequency ω_0. In the bipolaron case we consider electrons with opposite spin. The last two terms in Eq. (1) represent the on-site same-orbital (U_1) and different-orbital (U_2) Coulomb repulsion. For simplicity we have chosen $U_1=U_2=U$.

Most of the calculations will be compared to a simpler Holstein model:

$$H=-t\sum_{i,s}\ (c^+_{i+1,s}c_{i,s}+\ \text{H.c.})+\omega_0\sum_i\ a_i^+a_i$$

$$+g\omega_0\sum_{i,s}\ n_{i,s}(a_i^++a_i)+U\sum_i\ n_{i,\uparrow}n_{i,\downarrow}\,. \qquad (2)$$

While the basic principles of the method have been explained elsewhere,[13,25] here we present only a brief explanation of how the variational space is constructed for the case of two electrons in the JTM. Basis states for the many-body Hilbert space can be written $|\phi\rangle=|j_1,o_1,j_2,o_2;\ldots n_i,n_{i+1}\ldots m_i,m_{i+1}\ldots\rangle$, where j_1,j_2 and o_1,o_2 are first and second electron site and orbital indices, respectively, and there are n_i phonons of type a and m_i phonons of type b on site i. A variational subspace is constructed beginning with an initial state where both electrons are on the same site and orbital with no phonons, and operating repeatedly (N_h times) with the off-diagonal pieces (t and g) of the Hamiltonian [Eq. (1)]. The wave function is then written in a translation invariant form. To achieve high accuracy in the strong-coupling limit where there are many excited phonon quanta, we have constructed towers of N_{ad} ($N_{ad}=30$ for the JTM and $N_{ad}=200$ for the HM) additional phonon excitations (for the JT case: one tower for each phonon type) that were located on the electron site and on the first neighbor site to the left *or* to the right of the electron position. Such towers play a crucial role in achieving convergence in the small polaron regime.

III. JAHN-TELLER POLARON

A. Static correlation functions

We start by presenting results of the JT polaron (JTP). To investigate the shape of the JTP, we have computed various static correlation functions. We first present the correlation function for the distribution of the number of excited phonons in the vicinity of the electron,

$$\gamma(i-j)=\langle\psi_k|n_i(a_j^+a_j+b_j^+b_j)|\psi_k\rangle, \qquad (3)$$

where $n_i=n_{i,1}+n_{i,2}$ and $|\psi_k\rangle$ is the polaron wave function at momentum k. Numerical results presented in Fig. 1 show $\gamma(i-j)$ calculated at various coupling strengths and different wave numbers. When comparing results at different k it becomes evident that the size of the polaron at $k=\pi$ is larger than that at $k=0$. As the coupling strength increases, $\gamma(0)$ increases while $\gamma(i-j\neq 0)$ does not change substantially at $k=0$ while for larger values of k, $\gamma(i-j\neq 0)$ slightly decreases. We should stress that due to the the symmetry of the pseudospin rotation,[26] $\langle\psi_k|n_ia_j^+a_j|\psi_k\rangle=\langle\psi_k|n_ib_j^+b_j|\psi_k\rangle$. In Fig. 1 we also compare JTP with the Holstein polaron (HP), where γ is calculated at $g=1.2$. While differences at small k are very subtle, they become more pronounced at larger k where $\gamma(0)$ of the HP is larger than that of the JTP.

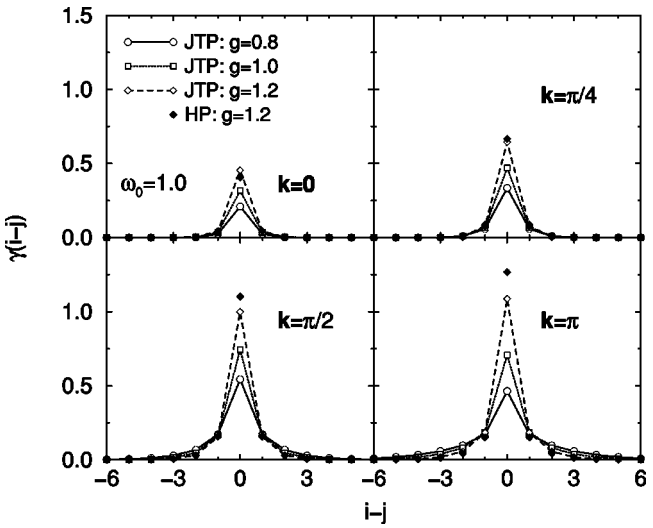

FIG. 1. $\gamma(i-j)$ vs $(i-j)$ for the JTP calculated at three different coupling strengths and $\omega_0=t=1$ (open symbols). Results for the HP are presented as black diamonds.

Next we present the phonon-phonon correlation function of the JTP,

$$\varepsilon(i-j)=\langle\psi_k|a_i^+a_ib_j^+b_j|\psi_k\rangle, \qquad (4)$$

shown in Fig. 2. As expected, phonons of two different types are only weakly correlated. At small values of k the electron mediated phonon-phonon interaction is always attractive [it has a maximum at $(i-j)=0$], however, at larger values of k and in the weak to intermediate coupling regime it becomes repulsive [$\varepsilon(i-j)$ peaks at $(i-j)=\pm 1$]. In contrast, the expectation for the same phonon type, $\langle\psi_k|a_i^+a_ia_j^+a_j|\psi_k\rangle$, always peaks at $(i-j)=0$ (not shown).

The static correlation function between the electron position and the oscillator displacement is defined as

$$\chi(i-j)=\langle\psi_k|n_i(a_j^++a_j)|\psi_k\rangle. \qquad (5)$$

We should stress that when using properly symmetrized ground-state wavefunction in the pseudo-spin space, we numerically obtain the following equality: $\langle\psi_k|n_i(b_j^++b_j)|\psi_k\rangle=\langle\psi_k|n_i(a_j^++a_j)|\psi_k\rangle$. In Fig. 3 we present $\chi(i-j)$ in the intermediate coupling regime, i.e., $g=1$. At $k=0$, where the group velocity is zero, the deformation around the electron position is limited to only a few lattice sites, $\chi(i-j)$ is always positive and seems to be exponentially decaying. At finite but small $k=\pi/4$, the local defor-

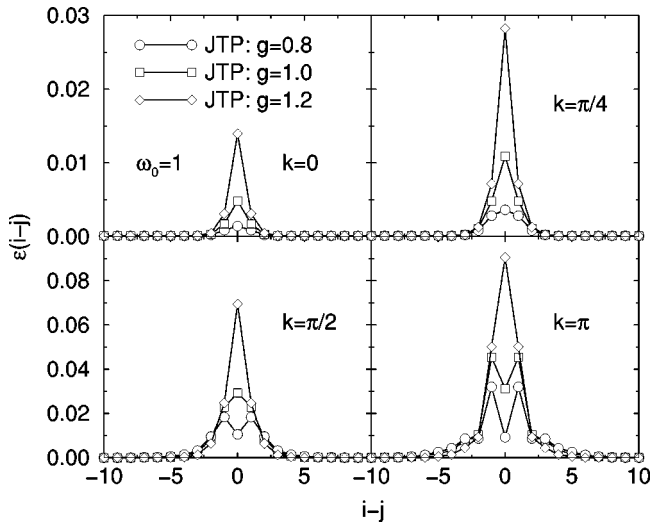

FIG. 2. $\varepsilon(i-j)$ vs $(i-j)$ calculated at three different coupling strengths and $\omega_0=t=1$. Note that vertical scales are different for $k=0,\pi/4$ and $k=\pi/2,\pi$.

mation around the electron increases in amplitude. We also notice a ringing effect (oscillating deformation) as a consequence of a finite velocity at $k\neq 0$. At $k=\pi/2$ the ringing effect is strongly enhanced while the spatial extent of the deformation increases in comparison to $k=0$. The range of deformation reaches its maximum at $k=\pi$ while at the same time the lattice displacement on the electron site decreases in comparison to smaller values of k. In comparison with the HP (also presented in Fig. 3), the main difference is in $\gamma(0)$ which in the case of the JTP diminishes strongly with increasing k.

An important advantage of defining the Hilbert space on an infinite lattice is in the ability to calculate the energy of the system E at arbitrary value of k. This makes our method extremely efficient for computing the effective mass of the polaron:

$$m^{*-1}=\left.\frac{\partial^2 E(k)}{\partial k^2}\right|_{k=0}. \tag{6}$$

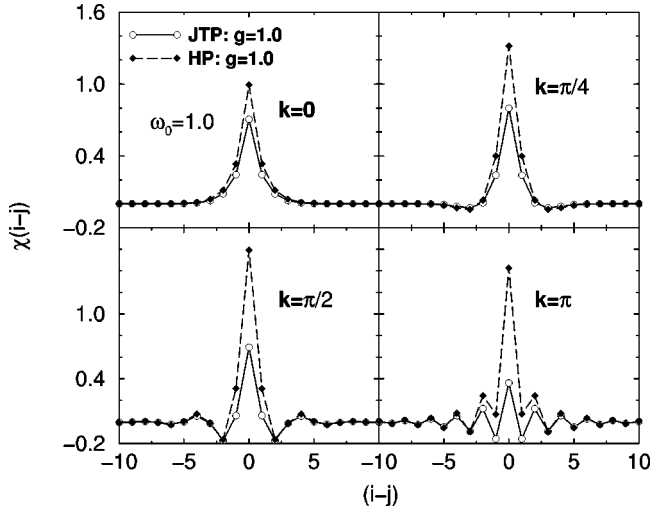

FIG. 3. $\chi(i-j)$ vs $(i-j)$ for the JTP and HP, $t=1$.

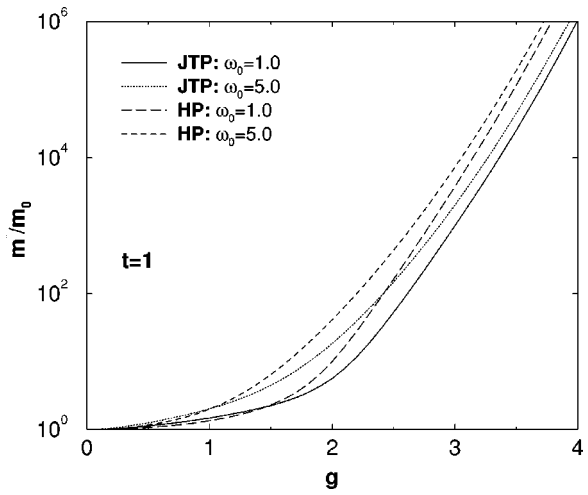

FIG. 4. Effective mass of the JTP and HP vs g for $t=1$, $\omega_0=1$ and 5.0, on a log scale.

The second derivative is evaluated by finite differences in the neighborhood of $k=0+dk$. Comparison between the JTP and HP effective masses is presented in Fig. 4. In accordance with the Kornilovitch results,[24] the effective mass of the HP polaron is smaller than the JTP in the weak to intermediate coupling regime. With increasing coupling the JTP becomes lighter than the HP. From Fig. 4 it seems as if the effective mass of the JTP and HP displays a similar behavior in the strong coupling limit.

The evolution of a polaron state with changing k can be inspected by calculating the quasiparticle weight and the mean phonon number N_k^{ph},

$$Z_k=|\langle\psi_k|c_k^\dagger|0\rangle|^2, \tag{7}$$

$$N_k^{ph}=\sum_i \langle\psi_k|a_i^\dagger a_i+b_i^\dagger b_i|\psi_k\rangle, \tag{8}$$

where $c_k^\dagger|0\rangle$ represents a state with an electron and no excited phonons and $|\psi_k\rangle$ is the solution of the model at finite k. Note that the difference between $Z_{k=0}$ and the inverse effective mass Eq. (6) comes from $k-$ dependence of the polaron self-energy $\Sigma(k,\omega)$.[14] At finite k, Z_k measures the electronic character of the polaronic wave function. In Fig. 5 we present Z_k and N_k^{ph} for the HP and JTP calculated at two different coupling strengths $g=0.7$ and $g=2.0$. Consistent with results for the effective mass in Fig. 4, Z_k of the JTP is slightly larger than the HP at $k=0$ and $g=2$. With increasing k we observe a smooth crossover from the predominantly electronic character (large Z_k) toward the phononic character (small Z_k) of a polaron. This crossover is sharper in the HP case as Z_k of the JTP intersects Z_k of the HP close to $k=0.3\pi$ $(g=0.7)$. This intersection is also reflected in N_k^{ph} even though N_k^{ph} does not differ substantially between the two models. In the case of large coupling, $g=2.0$, Z_k for the JTP is larger than Z_k of the HP, which is consistent with the behavior of the effective mass in the strong coupling regime. Moreover, N_k^{ph} of the JTP is substantially smaller than N_k^{ph} of the HP.

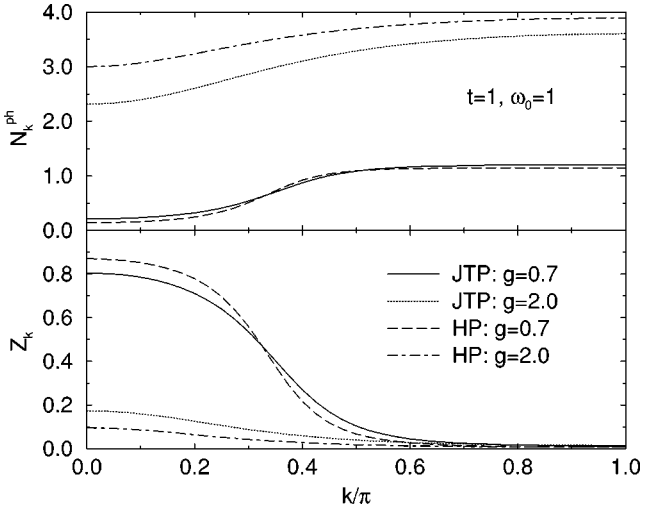

FIG. 5. N_k^{ph} (top) and Z_k (bottom) vs k/π for two different coupling strengths.

B. Optical conductivity

Applying standard linear-response theory, the real part of the conductivity takes the form (in the limit $T=0$)

$$\Re\sigma(\omega)=D\,\delta(\omega)+\sigma^{reg}(\omega>0), \tag{9}$$

where D is the Drude weight at $\omega=0$ and σ^{reg} is the finite-frequency response given by

$$\sigma^{reg}(\omega)=\pi e^2\sum_n \frac{|\langle\psi_0|J|\psi_n\rangle|^2}{E_n-E_0}\,\delta(\omega+E_0-E_n), \tag{10}$$

where all states $|\psi_n\rangle$ for $n=1,2,\ldots$ belong to $k=0$ space. It is important to stress that in Eq. (10), the current operator J has the same form in the Jahn-Teller and Holstein model:

$$J=-iet\sum_{i,o}\,(c^{+}_{i+1,o}c_{i,o}-\text{H.c.}). \tag{11}$$

Therefore, we should expect a similar behavior of $\sigma^{reg}(\omega)$ in both models. We next introduce the ω-integrated spectral weight,

$$S^{reg}(\omega)=\int_{0^+}^{\omega}\sigma^{reg}(\omega)d\omega, \tag{12}$$

and arrive at the sum rule

$$S^{tot}=\frac{\pi e^2}{2}\langle -H_{kin}\rangle=S^{reg}+\pi e^2 t m^{*-1}, \tag{13}$$

where $S^{reg}=S^{reg}(\infty)$. The sum rule may be used to test the numerics by calculating the effective mass by first using Eq. (6) and second, Eq. (13). In all cases presented the numerical sum rules are satisfied to at least six digits.

While our numerical method, defined on the infinite lattice, enables us to keep the numerical precision in the thermodynamic limit of static correlation functions including m^*, S^{tot}, and S^{reg} within a linewidth, there are finite-size effects when presenting finite-frequency quantities. The reason is that the obtained spectrum is discrete and we are thus forced to use a small $\epsilon\sim 0.05$ to smooth the continued-fraction form of Eq. (10). On the other hand, the integrated spectral weight $S^{reg}(\omega)$ does not depend on ϵ and is thus more reliable.

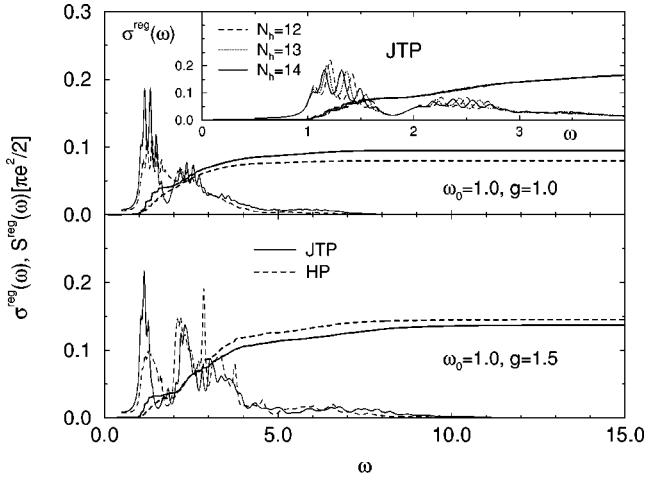

FIG. 6. $\sigma^{reg}(\omega)$ and $S^{reg}(\omega)$ vs ω for $g=1$ (top) and $g=1.5$ (bottom) for the JTP (full lines) and HP (dashed lines). The inset (top) shows $\sigma^{reg}(\omega)$ and $S^{reg}(\omega)$ for the JTP calculated at three sizes of the Hilbert space with $N_h=12$,13, and 14. Convergence of $S^{reg}(\omega)$ is within the linewidth.

We first present $\sigma^{reg}(\omega)$ and its integral $S^{reg}(\omega)$ in Fig. 6 for the JT and HM in the weak to intermediate coupling regime. The precision of our results in the thermodynamic limit can be tested in the weak coupling limit, where the optical conductivity threshold is known to be at $\omega=\omega_0$. In this case, other methods, defined on finite systems, show pronounced finite-size effects due to discreteness in k space which are reflected in the threshold, larger than ω_0 in the weak-coupling limit,[19–21] and rather well separated peaks corresponding to scattering of the initial $k=0$ electron state into finite-k states. The main signature of $\sigma^{reg}(\omega)$ at $g=1.0$ of both models (JT and HM) is that the spectra are strongly asymmetric in frequency, which is a characteristic of large polarons.[27] Both spectra seem to share the same threshold frequency ω_0.[28] The first two broad peaks are due to one- and two-phonon emission processes. Peaks are more pronounced in the JT than in the HM case. With increasing coupling g, $\sigma^{reg}(\omega)$ of both models shifts toward higher frequencies and remains similar. The threshold frequency does not change significantly.

We feel obliged to discuss the constraint of the finite Hilbert space effects on the presented spectra in more detail. In the inset of Fig. 6 we present $\sigma^{reg}(\omega)$ for the JTP calculated for three different sizes of the Hilbert space. We can clearly see that broad features (two broad peaks) in $\sigma^{reg}(\omega)$ converge rather well; however, the number and position of small peaks that compose broad peaks change slightly with increasing N_h. Excited states that contribute to $\sigma^{reg}(\omega)$ in the total $k=0$ sector can be represented as a polaron with the wave vector k_p and excited phonon or phonons with the total wave vector $k_{ph}=-k_p$. Small peaks therefore represent a scattering of the polaron into different k_p states with one- or multiple-phonon emissions. Since in our variational space

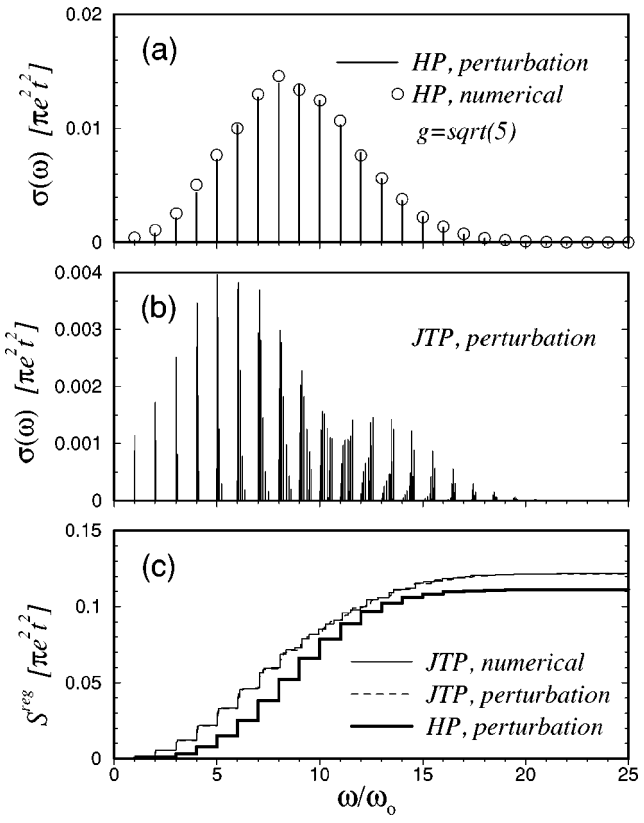

FIG. 7. Optical conductivity: second-order perturbation theory is compared with the numerical result. The height of the peaks represents the weight of the δ functions. The numerical calculations are performed on the two-site Holstein or Jahn-Teller models with $t=0.05$ and $\omega_0=1$. The electron-phonon coupling is $g=\sqrt{5}$ for all panels.

phonons are allowed only N_h steps away from the electron, there are only discrete k_p's allowed for such scattering. In the inset of Fig. 6 we also present the integrated conductivity $S^{reg}(\omega)$ for the same sizes of the Hilbert space. The convergence in this case is excellent.

For small hopping t, one can readily calculate optical conductivity $\sigma^{reg}(\omega)$ using strong-coupling perturbation theory, i.e., the Lang-Firsov transformation. For a two-site Holstein model,[29] we have

$$\sigma^{reg}(\omega)=\sum_{n=1}^{\infty}\sigma_n\delta(\omega-n\omega_0)$$
$$=\pi e^2t^2e^{-2g^2}\sum_{n=1}^{\infty}\frac{(2g^2)^n}{n!n\omega_o}\delta(\omega-n\omega_0)+O(t^4). \tag{14}$$

We note that $\sigma^{reg}(\omega)$ is not quite Poisson distributed. It is composed of a series of Dirac δ functions centered at the frequencies $\omega=n\omega_o+O(t)$. Their weights σ_n are second order in t. For $g\gg1$, the largest σ_n in Eq. (14) occurs when $n=2\omega_0(g^2-1)\sim2E_p$, which is consistent with previous numerical studies.[22] Figure 7(a) shows good agreement between perturbation theory and the numerical result.

In contrast, applying perturbation theory to the JTP is much more difficult because the single-site problem does not have an exact solution. Reasonably accurate trial wave functions for the low-lying levels have been proposed.[30,31] However, obtaining the analytic wave functions for the whole spectrum remains an arduous task. In the following, we evaluate the second-order perturbation based on the numerically exact solutions of the single-site problem. It is known that the eigenfunctions $\phi_{n,j}$ of a JT site are characterized by the radial quantum number n and the angular quantum number j. Each state is doubly degenerate and $n=0$, $j=\pm1/2$ for ground states. Thus, for a two-site JTP we chose the ground state to be

$$|\psi_0\rangle=\frac{1}{\sqrt{2}}[c_1^\dagger|\phi_{n,1/2}\rangle|0,0\rangle+c_2^\dagger|0,0\rangle|\phi_{n,1/2}\rangle], \tag{15}$$

where $|0,0\rangle$ is the phonon state on the site without the electron. We have

$$\sigma^{reg}(\omega)=\pi e^2t^2\sum_{n,m_1,m_2=0}^{\infty}\frac{|\langle\phi_n|0,0\rangle\langle m_1,m_2|\phi_0\rangle|^2}{E_n-E_0+(m_1+m_2)\omega_0}$$
$$\times\delta[\omega-E_n+E_0-(m_1+m_2)\omega_0]+O(t^4), \tag{16}$$

where E_n is the eigenvalue of ϕ_n and $n+m_1+m_2>0$. The quantum number j is left out because it is conserved by current operator. All the nonzero matrix elements exist only between states with $j=1/2$. In addition, the radial excitation of the JTP is anharmonic due to its Mexican-hat potential surface. *Therefore, the δ function peaks are not necessarily located near $n\omega_0$.* We illustrate the distinct feature in Fig. 7(b), in which the anharmonicity manifests itself clearly when the excited states come near the cone of the Mexican-hat potential. (The height of the cone is $g^2\omega_0$ measured from the bottom of the potential surface.) There are actually two peaks near ω_0 and three peaks near $2\omega_0$ because the excited phonon quanta can either be harmonic or anharmonic. An excellent agreement between perturbation theory Eq. (16) and Lanczos diagonalization is found in Fig. 7(c). Although the total weight of the JTP and HP are approximately equal, in the low-frequency regime, we note that $S^{reg}_{JTP}(\omega)\gg S^{reg}_{HP}(\omega)$ as a result of the fact that the JTP has a larger quasiparticle weight than the HP.[26,31]

Turning to the sum rules presented in Fig. 8, we notice a monotonic decrease of the total sum rule S^{tot}, which indicates a suppression of the electronic kinetic energy in the strong coupling regime. The drop in S^{tot} is accompanied by a decrease in the Drude weight D, which is a measure of the coherent transport properties of a polaron. Although the decrease is less steep in the JTP case, the two models show strong similarities. The dependence of the regular part S^{reg} of the optical conductivity, which measures the dissipative part of $\sigma(\omega)$, is not monotonic in the electron phonon coupling g. It first increases with increasing g, reaches the peak near the crossover from large to small polaron regimes and then decreases with further increase of g. Such an enhancement of S^{reg} in the intermediate coupling regime has already

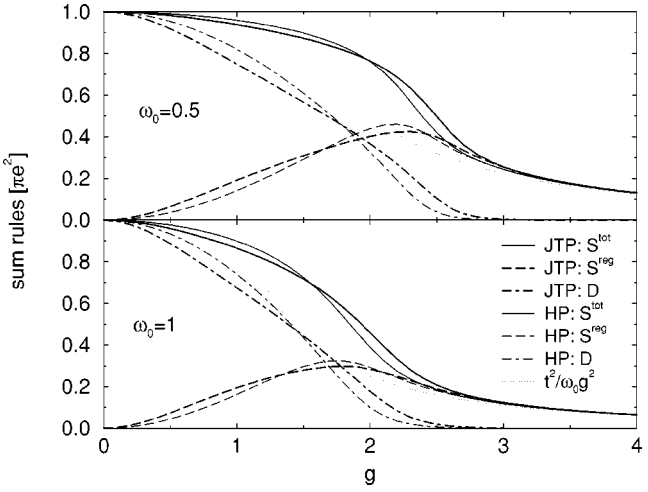

FIG. 8. Partial and total sum rules for $\omega_0=0.5$ (top) and $\omega_0=1.0$ (bottom) as a function of coupling g, $t=1$. Thicker lines represent JTP results, thinner lines HP results. The thin dotted line is a strong coupling result.

been observed in the Holstein case.[19] In the strong coupling limit S^{tot} of *both* models approach the asymptotic value $S^{tot}\sim t^2/\omega_0 g^2$ (see Fig. 8), which can be obtained by integrating Eq. (14) and summing over all phonon excitations in the limit $g\gg\omega_0$. It is rather surprising that even though the strong coupling expansion is in principle not valid for the JT case, S^{tot} for the JT model seems to approach the same asymptotic behavior. All quantities in Fig. 8 have an error of less than a linewidth.

IV. BIPOLARON

The following section does not apply to manganites, since the strong Hund's rule coupling renders JT bipolarons unbound. It does, however, apply to other transition-metal oxides with filled t_{2g} shells, such as Ni or Co. As we will see in this section, similarities between the JT and Holstein models persist in the case of two electrons. We start by comparing the electron-electron correlation function

$$C(i-j)=\langle\psi_k|n_i n_j|\psi_k\rangle, \tag{17}$$

where $n_i=n_{i,1}+n_{i,2}$ and $|\psi_k\rangle$ is the bipolaron wave function at momentum k. In Figs. 9(a) and 9(b) we present $C(i-j)$ for $k=0$ and different values of the electron-phonon and Coulomb interactions. For $U=0$ the JT bipolaron (JTB) and Holstein bipolaron (HB) show very small differences. At smaller coupling $g=1$, Fig. 9(a), the effect of increased U on the JTB and HB is similar. The main effect of finite U is to enlarge the size of the bipolaron, caused by the electrons trying to avoid double occupancy. At a slightly larger coupling $g=1.3$ [Fig. 9(b)], the effect of finite U is slightly more pronounced in the case of JTB than HB. We can conclude that the JTB in the intermediate to strong coupling regime has a slightly larger radius at finite U than the HB.

A larger radius of the bipolaron should imply a larger mobility of the bipolaron. It is known that in the HB, with increasing U the on-site bipolaron transforms into an intra-

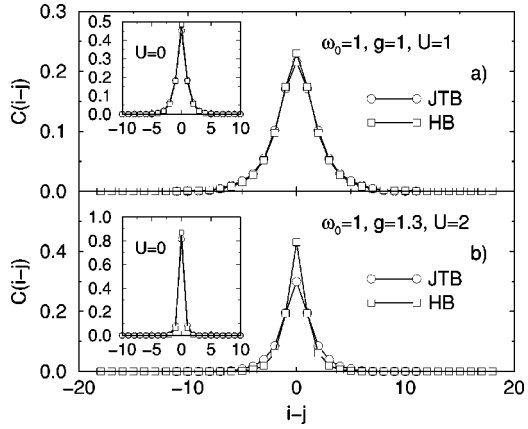

FIG. 9. $C(i-j)$ vs $i-j$. We have used $N_h=18$ for the HB and $N_h=11$ for the JTB.

site bipolaron with a reduced effective mass.[25,32,33] We may therefore expect the JTB to have a smaller effective mass than the HB due to a larger radius observed in Fig. 9(b). This indeed turns out to be the case as seen in Fig. 10, where we show the bipolaron effective mass vs U in units of the polaron mass for two different coupling strengths. We see that JTB effective mass is smaller than HB effective mass by up to a factor of 2 for all U and for both coupling strengths. As shown in the inset of Fig. 10, the JTB at $g=1.3$ has a smaller binding energy than the HB, corresponding to its larger radius and smaller mass. The binding energy is defined as $\Delta=E_{bi}-2E_{po}$, where E_{bi} and E_{po} are bipolaron and polaron ground-state energies, respectively.

We conclude our numerical investigation of the JTB with the phase diagram presented in Fig. 11 for the transition from unbound polarons to bound bipolarons. We have obtained the phase diagram using the condition $\Delta(U,g)=0$. It is important to stress that a bound bipolaron exists in both models at $U=0$ and at any finite g. In the weak coupling limit, i.e., $g\ll 1$, the phase boundary is given by $U_c=2\omega g^2$, represented by the dashed line in Fig. 11. This result can be derived in the classical limit and it is identical for both the JT and H

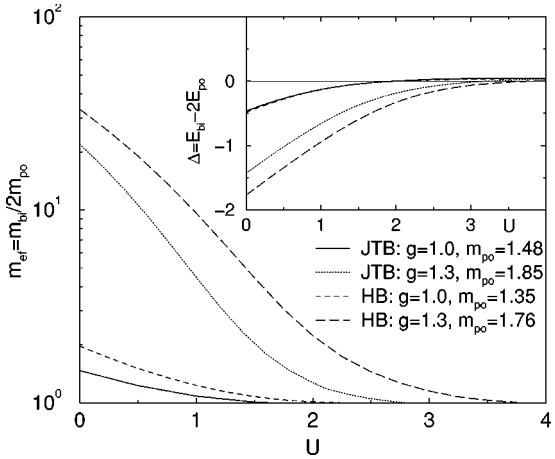

FIG. 10. Effective mass of JTB and HB results vs U for $\omega_0=1.0$. Inset: JTB and HB binding energies vs U. Finite-Hilbert space scaling was used for better accuracy.

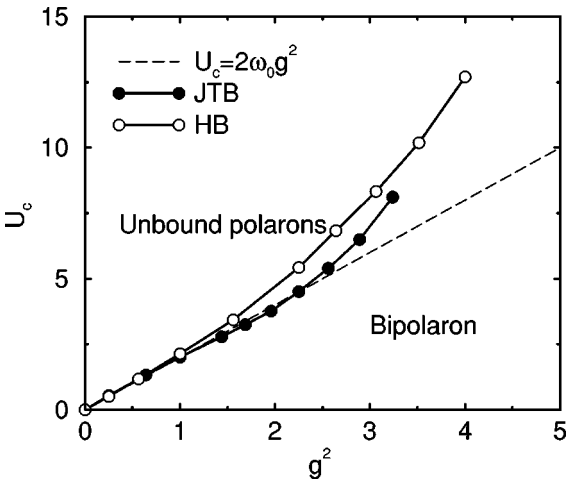

FIG. 11. The phase boundary between two separate polarons and a bipolaron calculated for $\omega_0=1$.

models. With increasing g, the JTB phase boundary deviates slightly downward from the given analytical estimate, while for the HB it deviates upward. Approaching the strong coupling regime, $U_c(g)$ for the JTB seemingly approaches the phase boundary of the HB which in the strong coupling regime follows $U_c=4\omega_0 g^2$.[25] Due to the large Hilbert space of the JTB were unable to investigate the strong coupling regime of the JTB more precisely in order to determine weather the two phase boundaries merge with increasing g.

V. CONCLUSIONS

We have performed a detailed numerical analysis of the JTM in one spatial dimension. The main conclusion is that the simple $E\otimes e$ JTM is, despite extra orbital and phonon degrees of freedom, very similar to the Holstein model (although the former has a doubly degenerate ground state and the latter does not). This result agrees with recent quantum Monte Carlo calculations[24] and analytical comparison of both models.[26] Closer examination reveals that the effective mass of the JTM is larger than HP effective mass in the weak coupling regime and smaller by roughly a factor of g in the strong coupling regime, where the effective masses of JTP and HP share the same exponent.

Turning to spectral properties, our numerical method gives extremely reliable results for $\sigma^{reg}(\omega)$, which can be seen in weak to intermediate coupling by observing the threshold frequency (the gap in the spectra). This agrees with the weak-coupling prediction, i.e., $\omega_{tr}=\omega_0$. We also support this claim by providing $\sigma^{reg}(\omega)$ for systems with different numbers of variational states. $\sigma^{reg}(\omega)$ at $g=1.0$ clearly shows two broad peaks corresponding to one- and two- phonon emission. These peaks are much more pronounced in the JTM than in the HM. In the strong coupling regime, we find excellent agreement of $\sigma^{reg}(\omega)$ for the Holstein model with a simple Lang-Firsov strong coupling analytical expression. However, the spectrum of the Jahn-Teller polaron is qualitatively different. Due to the anharmonicity of its radial phonon excitation, the peaks of $\sigma^{reg}(\omega)$ are not necessarily located near the multiples of ω_0. For both models, the sum rule in this regime is given by $S^{tot}\sim t^2/\omega_0 g^2$.

Strong similarities between HM and JTM also persist in the case of two bound polarons. Similar to the one polaron case, the Jahn-Teller bipolaron has a smaller effective mass than Hubbard bipolaron in intermediate coupling independent of the strength of U. This is mostly a consequence of smaller binding energy.

ACKNOWLEDGMENTS

J.B. gratefully acknowledges the support of Los Alamos National Laboratory where part of this work was performed, the financial support by the Slovene Ministry of Science, Education and Sport. This work was supported in part by the U.S. DOE and by LANL LDRD.

[1] A. J. Millis, P. B. Littlewood, and Boris I. Shraiman, Phys. Rev. Lett. **74**, 5144 (1995).
[2] G.-M. Zhao *et al.*, Nature (London) **381**, 676 (1996).
[3] M. Quijada, J. Černe, J. R. Simpson, H. D. Drew, K. H. Ahn, A. J. Millis, S. Shreekala, R. Ramesh, M. Rajeswari, and T. Venkatesan, Phys. Rev. B **58**, 16 093 (1998).
[4] A. Moreo *et al.*, Science **283**, 2034 (1999).
[5] V. Brouet, H. Alloul, Thien-Nga Le, S. Garaj, and L. Forró, Phys. Rev. Lett. **86**, 4680 (2001).
[6] O. Gunnarsson, Phys. Rev. B **51**, 3493 (1995).
[7] A. Auerbach, N. Manini, and E. Tosatti, Phys. Rev. B **49**, 12 998 (1994).
[8] N. Manini, E. Tosatti, and A. Auerbach, Phys. Rev. B **49**, 13 008 (1994).
[9] M. Capone, M. Fabrizio, P. Giannozzi, and E. Tosatti, Phys. Rev. B **62**, 7619 (2000).
[10] F. Marsiglio, Physica C **244**, 21 (1995).
[11] G. Wellein, H. Röder, and H. Fehske, Phys. Rev. B **53**, 9666 (1996); G. Wellein and H. Fehske, *ibid.* **56**, 4513 (1997); **58**, 6208 (1998); A. Weise, H. Fehske, G. Wellein, and A. R. Bishop, *ibid.* **62**, R747 (2000).
[12] E. V. L. de Mello and J. Ranninger, Phys. Rev. B **55**, 14 872 (1997).
[13] J. Bonča, S. A. Trugman, and I. Batistič, Phys. Rev. B **60**, 1633 (1999).
[14] Li-Chung Ku, S. A. Trugman, and J. Bonča, Phys. Rev. B **65**, 174306 (2002).
[15] H. De Raedt and A. Langedijk, Phys. Rev. Lett. **49**, 1522 (1982); Phys. Rev. B **27**, 6097 (1983); **30**, 1671 (1984).
[16] P. E. Kornilovitch and E. R. Pike, Phys. Rev. B **55**, R8634 (1997).
[17] A. W. Romero, D. W. Brown, and K. Lindenberg, J. Chem. Phys. **109**, 6540 (1998).
[18] E. Jeckelmann and S. R. White, Phys. Rev. B **57**, 6376 (1998).
[19] H. Fehske, J. Loos, and G. Wellein, Z. Phys. B: Condens. Matter **104**, 619 (1997).
[20] M. Capone, W. Stephan, and M. Grilli, Phys. Rev. B **56**, 4484

(1997).
[21] H. Fehske, J. Loos, and G. Wellein, Phys. Rev. B **61**, 8016 (2000).
[22] A. S. Alexandrov, V. V. Kabanov, and D. K. Ray, Physica C **224**, 247 (1994).
[23] Chunli Zhang, E. Jeckelmann, and S. R. White, Phys. Rev. B **60**, 14 092 (1999).
[24] P. E. Kornilovitch, Phys. Rev. Lett. **84**, 1551 (2000).
[25] J. Bonča, T. Katrašnik, and S. A. Trugman, Phys. Rev. Lett. **84**, 3153 (2000).
[26] Y. Takada, Phys. Rev. B **61**, 8631 (2000).
[27] D. Emin, Phys. Rev. B **48**, 13 691 (1993).
[28] At strong coupling, the Jahn-Teller polaron has phonon excitations at much lower frequency than ω_0 (angular excitations of the Mexican hat), but these cannot be accessed optically for the type of hopping considered here.
[29] It can be shown that for N sites ($N>2$) with periodic boundary conditions, the result of the perturbation is approximately a factor of 2 larger than that of the two-site model.
[30] I. B. Bersuker and V. Z. Polinger, *Vibronic Interactions in Molecules and Crystals* (Springer, Berlin, 1989).
[31] L.-C. Ku, S. A. Trugman (unpublished).
[32] A. La Magna and R. Pucci, Phys. Rev. B **55**, 14 886 (1997).
[33] L. Proville and S. Aubry, Physica D **133**, 307 (1998); Eur. Phys. J. B **11**, 41 (1999); **15**, 405 (1999).